

• **U.S. GOVERNMENT CONTRACTORS:**

Work prepared by authors under a contract for the U.S. Government (e.g., U.S. Government labs) may or may not be subject to copyright transfer. Authors must refer to their contractor agreement. For works that qualify as U.S. Government works by a contractor, ASCE acknowledges that the U.S. Government retains a nonexclusive, paid-up, irrevocable, worldwide license to publish or reproduce this work for U.S. Government purposes only. This policy DOES NOT apply to work created with U.S. Government grants."

1 **Landslide analysis of historical urban walls:**
2 **the case study of Volterra.**

3 M.L. Puppio⁽¹⁾, E. Vagaggini⁽²⁾, L. Giresini⁽³⁾, M. Sassu⁽⁴⁾

4 ⁽¹⁾ Department of Civil, Environmental Engineering and Architecture, University of Cagliari, Via Marengo
5 2, Italy, mariol.puppio@unica.it

6 ⁽²⁾ Department of Civil, Environmental Engineering and Architecture, University of Cagliari, Via Marengo
7 2, Italy, emma.vagaggini@gmail.com

8 ⁽³⁾ Department of Civil and Industrial Engineering, University of Pisa, Largo Lazzarino 1, Italy,
9 linda.giresini@unipi.it.

10 ⁽⁴⁾ Department of Civil, Environmental Engineering and Architecture, University of Cagliari, Via Marengo
11 2, Italy, msassu@unica.it.

12
13 **Abstract**

14 This work arises from the evidences of recent collapses of historical urban walls. These events, mainly
15 occurred after severe rainfalls, recalled the attention on the vulnerability of these infrastructures. Specific
16 evaluation models which take into account the role of moisture inside the walls are not frequent in the
17 literature. The problem is difficult to treat in many practical cases, due to the extension of the urban walls
18 and the variability of their geometry and of their mechanical features.

19 The integrity of the urban walls is investigated throughout the analysis of a set of vertical sections. Risk
20 scenarios of rainfall events are analysed. At this scope, four Limit States are proposed and investigated to
21 determine both collapse and serviceability conditions. The combined risk analysis is obtained by treating
22 the single-risk analysis. The results from the limit analysis are compared with those from the FEM models.
23 The method is applied to the relevant case study of the Volterra historical urban walls with a retrospective
24 analysis of the section which collapsed in January 2014 and the analysis of other relevant sections.

25 **Keywords:** historical urban walls; survey; vulnerability assessment; landslide vulnerability; hydraulic risk;
26 Volterra's urban walls.

28 **1 Introduction**

29 Recent failures occurred in the last years recalled expertise attention on the collapse of historical city walls.
30 In the last ten years a relevant number of defeats or collapse events of historical city walls took place in
31 Tuscany Region (Italy) (Puppio et al., 2019), (Andreini et al., 2013).

32 The investigation of those collapses shows that the presence of moisture inside the walls and the
33 surrounding soil due to several causes (rain, water losses etc.) as well as poor maintenance activities and
34 inadequate restoration works played a relevant role. This forced to introduce the effect of rainfalls and
35 moisture in the safety evaluation of the walls.

36 The current Italian Code provides indication for the natural actions induced by wind, earthquake, thermal
37 effects but not specifically by the presence of moisture. This is not easy to implement because of the fact
38 that humidity depends not only from extreme events as rainfalls, but also from permanent conditions such
39 as type of soil, drainage systems and human interferences.

40 In Geotechnics two limit scenarios are traditionally considered: the drained and undrained conditions. The
41 approach is related to the soil type and the rate of load application (permanent loads vs total loads). The
42 additional effect of water is usually considered in terms of hydraulic thrust and internal pore pressure.

43 The decay of the soil mechanical properties due to rainfalls is often neglected in common professional
44 cases. The actual method of modelling (Casapulla, 2008; Grillanda et al., 2019) and retrofitting of the
45 existing masonry buildings (Mistretta et al., 2019; Sassu et al., 2017) is usually affected by complexity and
46 a lot of uncertainties. Actually the rocking and cinematic approach (Casapulla C., Maione A., 2017;
47 Casapulla, 2015; Casapulla et al., 2010) is able to provide adequate indication about the safety of the wall
48 but the presence of the earth filling produces additional non linearity in the response. Nevertheless, taking
49 into account the weakening effect of the water plays a crucial role as showed below. The method presents
50 a general application which can also be applied to different cases and different sources of imbibition.

51 Urban walls are usually situated along the external perimeter of the historical centre of the old cities. They
52 were constructed both with commercial and defence functions. They also covered the static function of
53 retaining walls in case of slope. Those several aspects led to irregular shapes of the walls both in plan and
54 elevation (Y.C. Chan, 1982). The need to develop a method for survey and analysis should also consider
55 the influence of the water behind the walls. Numerical application is performed on Volterra urban walls
56 based on a set of collapsed sections.

57 The paper is structured in five section. Section 2 highlights some recent collapses and illustrates a survey
58 procedure to detect mechanical and geometrical parameters. In Section 3 a method to evaluate the effect of
59 rainfall infiltrations with different literature contribution is proposed. In this Section the assessment of the
60 hydraulic vulnerabilities is carried out considering the effect of weakening due to water imbibition. In
61 Section 4 the results are discussed.

62 **2 Collapses and survey strategy**

63 Tuscany Region (Italy) was affected in the last ten years by several collapses of historical urban walls:
64 seven examples on five different locations are summarized in Fig.1 and Tab.1.

65 In the investigated cases the presence of internal moisture and heavy rainfalls were recurring
66 events during the failure. The repairing costs resulted considerably high, respect to preventive maintenance
67 activities (an overall ratio of about 10/1), provided the other indirect costs, so the prevention based on
68 vulnerability assessment would lead to a significant loss reduction for the community.

69 The proposed survey methodology consists of the following steps:

- 70 (1) identification of a set of relevant vertical sections of the city walls;
- 71 (2) on-site geometrical survey;
- 72 (3) on-site mechanical assessment;
- 73 (4) extension of the results to the entire perimeter of the city walls.

74 The description of the survey procedure is reported in (Puppio et al., 2019; Vagaggini, 2019),
75 throughout the elaboration of on-site surveys with GIS data. The mentioned method is illustrated referring
76 to the collapses of the Volterra's city walls. Nowadays it preserves a historical city center of Etruscan origin
77 with a satisfactory state of conservation. The Etruscan portion of the walls is a part of these walls and the
78 arch of access to the city center is a masterpiece of priceless beauty.

79 The discretization of the perimeter (Puppio et al., 2019) is shown in Fig.2. The Middle Age walls enclose
80 the city centre and represent the core of this work. The surveyed sections on which the work is focused are
81 shown in red and blue in Fig. 2 and Fig.3. (0 / 78 and 86 /107), representing the Middle Age portions of
82 walls. The sections in blue in Fig. 2 are remains of the ancient Etruscan circuit of the walls.

83 On January 31st 2014, about 35 meters of the walls of Volterra collapsed in the area between “Porta
84 dell’Arco” and “Piazza dei Fornelli”. In this section the walls in front of “Via Lungo le Mura” are 9.5

85 meters high with the role of retaining structure, loaded by the upstream ground of about the entire height
86 of the wall. The moisture probably emphasized the reduction of bearing capacity of the walls.

87 Evidences of the effects of humidity appeared on the external face of the wall (Fig. 4) before the
88 failure. The rainfall that forced the collapse was preceded by water infiltrations with an evident lack of
89 drainage in the walls. The collapse exposed the foundations of adjacent buildings, as well as Palazzo Stella
90 (Fig.5). Non linear analyses taking into account an increasing level of hydraulic thrust were made in (Puppio
91 and Giresini, 2019). In this work, the weakening effect induced by water is instead neglected; the effect of
92 water is solely assumed as an additional thrust. The aging effect on blocks and mortar is also neglected,
93 since the collapsed portions of walls were of good masonry quality, as visible in Fig.6.

94 The main geotechnical and masonry parameters were investigated after the collapse. Two vertical
95 continuous drillings with Standard Penetration Tests (SPT) and three horizontal continuous drillings were
96 performed. The geological description is reported in (Santerecchi, 2014), whilst the geotechnical
97 parameters are recalled in Tab.2. To simplify the soil characterization, two main lithotypes were observed:
98 the Villamagna layer and the lime layer (Fig.7).

99 The Villamagna formation is made by a medium thick stratum of sand, interposed by a very weak
100 calcarenite layer; the lime layer just behind the wall is characterized by relevant inhomogeneity and poor
101 mechanical characteristics.

102 The GIS database furnished similar indications for the soil foundations, so the information of
103 Section 92-93 has been extended to the other vertical sections of the same typology. The collapsed section
104 (92-93) also furnished indications about the masonry features of the wall (Puppio and Giresini, 2019). It is
105 possible to identify two external layers made of sandstone irregular blocks, a porous rock typical of the site,
106 while the internal core was made by a mix of soil and small sand rocks from the nearby. Internal and
107 external parameters were not interconnected by diatons except for the top and the basement. Mechanical
108 parameters of the Volterra walls were obtained by the literature of masonry with similar features (D.M.
109 17/01/2018, 2018; Deere, 1988).

110 Along the perimeter of about 2,6 km, four emblematic sections have been chosen (Fig.8) for
111 geometric survey, to identify the most distinctive ones. These cross sections are emblematic due to the
112 following reasons:

113 1) geometric and mechanical data related to them are reliable;

- 114 2) geometric and mechanical properties of the selected cross sections are similar to many others
115 investigated along the walls perimeter;
- 116 3) the four cross-sections have all a soil backfill, so they are subjected to the highest horizontal
117 thrusts;
- 118 4) in these four cross-sections the highest percentage of vegetation and drainage with uncertain
119 effectiveness were found.

120 A partial survey was performed in other 25 sections to complete the geometrical assessment of the
121 perimeter. Concerning the adjacent areas around the walls, several buildings with at most four floors were
122 detected: the presence of buildings was then simulated by an extra load of 10 kN/m² for each floor.

123 The following conditions were observed during the survey:

- 124 (1) Upstream earth filling and inclined downstream face;
- 125 (2) Upstream earth filling and vertical downstream face;
- 126 (3) With no or partial filling and with a variable inclination of the downstream face;
- 127 (4) Upstream earth filling and vertical downstream face.

128 3 Analytical assessments of rainfall risk.

129 3.1 The model for soil weakened by rain.

130 Four specific Limit States (LS) have been defined: (1) Collapse (SLC), (2) Lifeguard (SLV), (3)
131 Damage (SLD) and (4) Integrity (SLI). These are similar to the ones provided for the buildings in the
132 European code in case of seismic action (Eurocode, 2004). In case of the retaining walls, those limit states
133 are given by the following values of the relative displacement d_r , defined by:

$$d_r = d_t - d_b \quad (1)$$

134 where d_t is the displacement of the top and d_b that of the basement (Fig.9).

135 The identification of the LS is conventionally carried out throughout the comparison with corresponding
136 displacements. Defining h_w as the height of the wall, it is possible to calculate the collapse displacement
137 d_{SLCg} by the condition of equilibrium, whilst lifeguard displacement d_{SLV} is equal to the 90% of the collapse
138 limit state one. Hence the retaining wall is essentially an isostatic structure d_{SLCg} depends on the first limit
139 failure mechanism (equilibrium of the isolate structure, equilibrium of the complex soil-wall, sliding, soil
140 limit capacity). This Ultimate LS can be calculated both with LEM or FEM methods. In particular the

141 overturning is calculated with the limit equilibrium method. The identification of d_{SLC} and consequently of
142 d_{SLV} is carried out, also depending on the actual boundary conditions of the section, thanks to limit and non-
143 linear analysis.

144 The displacement d_{SLD} corresponds to the damage of adjacent buildings, related to the maximum
145 displacements of the surrounding land. Finally, the displacement d_{SLI} can be defined, in aesthetic sense, by
146 the activation of the first crack on the wall or on the adjacent road pavement or on the plaster of adjacent
147 buildings. d_{SLI} have to be defined case by case according to the kind of masonry and the geometry of the
148 wall and of the surrounding area. This is not simple to estimate especially because of the complex
149 geometrical conditions and the variability of the kind of structure and infrastructure near the urban walls.
150 For this reason, an “Expert Judgement” is proposed as a strategy to identify this LS. The values of the
151 displacements for the four LS are summarized in Tab.3.

152 One of the triggering causes of collapse in historical walls is the presence of water. Ongoing variations in
153 rainfall quantity and intensity often causes landslides. The presence of water, from rainfalls or from other
154 sources, has a double effect: (1) reduction in the mechanical properties of soils, (2) increase of the hydraulic
155 thrust.

156 The SLIP model given by Montrasio and Yoshida (Montrasio and Valentino, 2016) is used to predict the
157 risk of landslides in an indefinite slope. This model, applied to recent case studies as in (Montrasio and
158 Valentino, 2007; Schilirò et al., 2016; Valentino et al., 2014), showed a good predictability level. In the
159 case of retaining walls, in order to estimate the effect of the decay of the mechanical parameters of soil
160 resistance from imbibition, the results of Montrasio and Yoshida (Yoshida et al., 1991) can be implemented.
161 This model is able to evaluate the reduction in shear strength, cohesion and friction angle of each soil layer
162 due to the increase of water penetration.

163 The SLIP Model given by Montrasio is applied to the case of the indefinite slope and doesn't consider the
164 reduction of the friction angle but only of the cohesion. The weakening effect of imbibition is given by
165 rain penetration and only superficial layers can be affected. The results of Yoshida allow to also take into
166 account the reduction of the friction angle. In addition, the discretization of the soil in horizontal strata
167 consents to consider the effects of imbibition in depth making the model also suitable for the evaluation of
168 the effects of the leaking of pipelines or other in depth sources of moisture. This differs with respect to the
169 application made by Montrasio that evaluates the effects of indefinite slope on soil surface.

170 It is usual to evaluate the landside safety by examining a series of failure surfaces. The effect of water
171 penetration can be considered by the equivalent saturation level: it depends on soil type, land use and
172 vegetal covering and on the intensity of rainfalls.

173 An improvement of the model creating a set of horizontal layers that can be damaged by rain penetration
174 is proposed. This modifies the overall strength and the consequent values of the defined LS.

175 Taken a portion of the soil of height H (Fig.10), the portion mH ($m < 1$) is completely saturated and the
176 remaining part $H(1-m)$ is partially saturated.

177 The percentage of saturation m can be expressed as follows:

$$m = \frac{\beta^* h}{n(1 - S_r)H} \quad (2)$$

178 where:

179 h height of rainfall;

180 H height of the soil interested by the rainfall;

181 β^* capacity of imbibition or percentage of filtered rain;

182 n soil porosity;

183 S_r saturation grade.

184 H depends on the presence of un-permeable soil layer. β^* can be estimated as 70% (Franceschini,
185 2012), (Losi, 2012).

186 The saturation grade is experimentally given by Montrasio et al. (Montrasio and Valentino, 2007)

187 as:

$$S_r(h) = S_{r0} + \frac{\beta h}{nH} \quad (3)$$

188 where S_{r0} is the initial saturation grade, β the capacity of imbibition and h is the height of rain. S_{r0} depends
189 on the initial moisture of the soil and consequently on the precipitation occurred in the days before the event
190 for the considered case of study. For the Volterra event it was assumed, given the soil characteristics from
191 in-situ tests, an initial saturation grade equal to 0,30.

192 The use of this model can also be applied to forecast what the intensity of the model that generate limit
193 scenarios is. It is an interesting way to evaluate the vulnerability of historical walls.

194 From equation (2) one can determine the depth of saturated soil mH which corresponds to a certain
195 height of rain h . It is well known that h is associated to rain duration and return period:

$$h = a d^k t^\eta \quad (4)$$

197 where t is the rain duration (expressed in hours), t_r is the return period of the event (expressed in years)
 198 (Fig.11). Dimensionless parameters a , κ , η are regional coefficients estimated by a multiple linear
 199 regression of regional rainfall record: for Volterra's site they can be found in (AA. VV., 2006). For each
 200 rain duration and return period a different imbibition scenario is then provided.

201 In the meanwhile, the shear resistance of the saturated layer is expressed by the well-known Mohr-
 202 Coulomb law:

$$\tau = c' + \sigma \tan \phi' \quad (5)$$

203 in which c' is the cohesion, ϕ' the friction angle and σ the compression stress.

204 The shear strength of the non-saturated soil is expressed in the model through a modified Mohr-Coulomb
 205 law:

$$\tau = c' + \sigma' \tan \phi' + c_\psi \quad (6)$$

206 where c_ψ is the initial apparent cohesion, as by Fredlund and Rahardjo in (Fredlund and Rahardjo, 1993)
 207 adding the positive effect of partial saturated soil. It can be expressed by:

$$c'_\psi = AS_r(1-S_r)^\lambda \quad (7)$$

208 where A and λ are dimensionless coefficients depending on the soil type. Both are identified by
 209 experimental tests by Montrasio and Valentino (Montrasio and Valentino, 2008), (Franceschini, 2012),
 210 (Montrasio et al., 2014), (Montrasio et al., 2009). For the sake of simplicity, the following value of c_ψ can
 211 be applied to the whole depth H :

$$c_\psi = c'_\psi (1-m)^\alpha \quad (8)$$

212 where α is the homogenization coefficient, here assumed equal to 3,40.

213 The variation of the apparent cohesion c_ψ with saturation is shown in Fig.12: in (b) shows that c_w quickly
 214 decreases with S_r for medium sands and tends to zero when S_r is higher than 80%. Also the friction angle
 215 varies with saturation as reported in (Farooq et al., 2015). The decreasing of the friction angle is proposed
 216 by Yoshida et al. (Yoshida et al., 1991). The variation of the specific weight of the soil depends on the soil
 217 porosity. All these variations, homogenised for the entire layers of height H , are listed in Tab.4.

218 3.2. Analysis of the landslide soil with rain penetration.

219 Two types of static analyses are carried out both for the hydraulic and the seismic vulnerability assessment:

- 220 • Limit Analysis Method (LAM);

221 • Finite Element Method (FEM).

222 The safety of a retaining wall is usually performed throughout the limit analysis method (LAM). The
223 analysis is here carried out using the SSAP2010 code (Borselli, 2018). LAM is a simplified method not
224 suitable to find all the limit states, for this purpose a FEM nonlinear static analysis is implemented in the
225 Straus 7 R.2.4. code (VV, n.d.). This takes into account the initial stress due to soil consolidation and the
226 internal pressure due to water and soil imbibition.

227 To the contrary, this approach is not applicable to the imbibition event. As a matter of fact, soil imbibition
228 can be related to external causes (such as leaking in water pipelines) and can maintain its consequences
229 over time, depending on rain duration, air moisture and soil type.

230 The following steps have been followed to perform the numerical analysis:

- 231 1) discretization of the soil surrounding the wall in horizontal layers of 100 cm;
- 232 2) definition of five different mechanical parameters for each layer during time, to simulate the
233 progressive effect of soil imbibition;
- 234 3) determination of the collapse load for the different limit states.

235 These steps are elaborated with an increasing height of rain which corresponds to different
236 imbibition scenarios.

237 The decay of the mechanical properties of the soil due to imbibition in horizontal layers is shown
238 in Tab.4. In Fig.13 the level of imbibition of each stratum is considered.

239 The SSAP2010 code for Limit Analysis implements the methods of Spencer (1967), Morgenstern & Price
240 (1965), Chen-Morgenstern (1983), Janbu (1967), Sarma I e II (1973). They can be applied on different shapes
241 and geometries of soil and structure. The output provides the surface failure characterized by the minimum
242 safety factor.

243 The FEM model by Straus 7 (without and with progressive imbibition) was determined involving a soil
244 area of about $4 h_w$ in plan and of about $2 h_w$ in elevation, with respect to the height of the wall (h_w). A series
245 of 100 cm soil layers permits to introduce the progressive presence of water penetration (Fig.14). The model
246 was created by 2-Dim plate elements with a max mesh size of 75 cm or 40 cm for the ground and masonry
247 respectively. Specifically, the masonry was an isotropic plane element, while the ground was a soil element.
248 A soil in situ stress is assigned to the soil as an initial condition to take into account the presence of the
249 adjacent buildings.

250 The plate elements are Quad-8 type, with 8 nodes (4 at the ends of the elements and other 4 at the middle
251 of the sides). Fig.14-16 represent the mesh of section 92-93. The different colours describe the property
252 plates; the upstream load simulates the buildings while the red lines inside each plate represent the soil in
253 situ stress applied to the soil.

254 The model is constrained laterally to fix horizontal movements along x , and at the base of the slopes to fix
255 the displacements along x and along y . The mechanical parameters are in Tab. 5 according to the Mohr-
256 Coulomb criterion.

257 As the height of rain increases with the duration, so does the saturation of the soil. This is reproduced
258 through six versions of the mesh which have an increasing number of soil layers (100 cm thick) involved
259 into the progressive decrease of the mechanical properties. These are summarized in Tab.6. Although the
260 initial properties of the soil are good, saturation has a remarkable effect in the reduction both of the cohesion
261 then of the friction angle. In fact, Tab. 7 shows a reduction of cohesion of -98% and of the friction angle
262 up to -39% varying the Saturation grade from 30% to 79% form for the material considered.

263 **3.3. Results**

264 In this section the results of the analysis carried out for the different sections are shown. Starting from the
265 collapsed section 92-93 the analyses are extended to the most relevant ones.

266 The corresponding results of FEM analysis, in terms of displacements and stresses for the
267 increasing load steps (code Straus 7 R.2.4.), are listed in Tab.7 and Fig.16.

268 The pushover analysis and principal stresses domain in case of rain duration of one hour
269 and a return period of 175 years is shown in Fig.17. This section, that is the one interested by the
270 collapse of January 2014, reveals the reduced safety factor also in dry condition. In particular the
271 application of the initial soil stresses in the FEM model is not possible for rain durations major
272 than 1 h because of the non-convergence of the models. So, a sensitivity analysis is carried out
273 considering the effective rain duration in the month before the collapse with the LAM model (Fig.
274 15).

275 Fig. 18 shows that the Safety Factor (SF) gets lower than one in an interval near the 29th of
276 January reaching a minimum value of 0.73 on the 12th of February if the collapse hadn't happened
277

278 before. It is possible to see that also a simple instrument such is the LAM method, can show a
279 great sensibility in predicting the vulnerability. In addition, it is interesting to highlight that the
280 minimum SF is reached a few days (12th of February) after the maximum height of rainfall is
281 registered (31st January), as an effect of imbibition in depth and retention capacity of the soil. This
282 work is extended to the most relevant sections presented in Fig.8 characterized by different
283 dimensions and boundary conditions.

284 In the following:

- 285 • Section 32-33 (Fig.19);
- 286 • Section 48-49 (Fig.20);
- 287 • Section 71-72 (Fig.21).

288 With the increase of rain duration, the most relevant failure mechanism for all the analysed
289 sections becomes the maximum displacement (d_{SLD}). Through the analysis of Fig.17-19 it was
290 possible to determine the rain duration that corresponds to this:

- 291 • Section 32-33: 1hour 50min;
- 292 • Section 48-49: 2hours 50min;
- 293 • Section 71-72: 2hours 20min;

294 Finally, considering a rainfall of 12 hours, the results for all the limit states are summarized in
295 Tab.7 with the determination of the corresponding return periods. It is then evident that the
296 capacity of the Volterra walls in section 92-93 was insufficient to sustain the rainfalls occurred
297 during the extraordinary climate events of January 2014. Tab.7 summarizes the results in terms
298 of return period and intensity measure for the four limit states analysed.

299 **4 Discussion**

300 All the sections analyzed in this paper are studied both with the FEM and the LAM method. FEM
301 allows a step by step evaluation of the stress and strain in the masonry and soil and provides a
302 good estimation of which the first mechanism of collapse to occur is.

303 The comparison between LAM and FEM Models shows that both are in good agreement in order
304 to provide indications about the collapse. In the analyzed case the presence of the filling and the

305 significant slope of the wall determine a global soil-wall failure. The presence of different levels
306 of imbibition involves different failure surfaces with the consequences of differentiate damages
307 to the adjacent buildings.

308 The site survey and the failure evidences have shown that degradation elements such as humidity,
309 vegetation, presence of buildings behind the wall can represent significant exposure elements.
310 Indeed, not only rainstorms can be considered as degradation phenomena but also persistent
311 humidity and filtrations caused by leak of pipelines are dangerous: in this sense a monitoring
312 system of moisture, consisting of a set of piezometers inside the soil, can be useful to prevent
313 degradation.

314 The retrospective analysis made for the collapsed section shows that in the case of Volterra the
315 application of the imbibition model, as modified in this work, provides interesting information
316 about the collapse happened and the possible cause. In particular, the reduction of the safety factor
317 highlights the great vulnerability of the collapsed section and the failure surfaces obtained by
318 SSAP and Straus 7 are close to the real one.

319 As the graphs of Fig.19-21 show the results are heavily dependent on the grade of imbibition.
320 Different saturation levels affect not only the Intensity Measure that generates a certain LS but
321 also the kind of failure that takes place first. The maximum damage displacement d_{SLD} is the first
322 to happen in case of an high imbibition level. Instead for a reduced grade of imbibition other
323 mechanisms are reached first. This suggests that the monitoring of displacements can provide
324 important information to prevent damage or failure. Intensity of the rain and rain duration are
325 both crucial variables.

326 This investigation is relevant in particular because of the “brittle failure” highlighted in real
327 collapse cases. The attaining of the first collapse mechanism (sliding, bearing capacity of the soil)
328 usually leads to the immediate failure of the retaining structure (dashed line on the curves). The
329 collapse also happens without warning and in an unexpected way. The sudden nature of this kind
330 of collapse is one of the most complex elements in the safety evaluation of ancient cities.

331 Possible countermeasures from engineering viewpoint could be the following, in ascending order
332 of impact to the construction:

- 333 a) increasing the drainage system to ensure a proper washout of rain and other sources of
- 334 water penetration, by new perforating holes distributed along the walls;
- 335 b) introducing passive steel tendons throughout the walls, to enforce the stabilization against
- 336 rocking movements;
- 337 c) introducing active steel wires tendons throughout the walls, anchored to visible steel
- 338 plates;
- 339 d) enforcing the basement of the wall through a reinforcement of the foundation or a set of
- 340 micropiles to avoid any slipping.

341 The improvement of the drainage systems, both with deep and on surface works (as rain runoff
342 and wastewater collectors and sub horizontal drains) is always recommended as shown here. In
343 addition, the adoption of early warning systems for monitoring the moisture by piezometers and
344 the relative displacements by inclinometers is a key strategy. The description of the mechanical
345 parameters of the walls in terms of Bayesian approach (Croce et al, 2021) could also help the
346 entire consolidation strategy.

347 This kind of analysis, in which vertical loads are incremented, shows some pushover curves that
348 differ from the common ones. In detail, the first part of the curves exhibits displacements that are
349 opposite with respect to those that lead to the collapse.

350 This is because of an initial consolidation effect induced by the increase of vertical pressures. The
351 effect is due to the geometry, in particular to the presence of the upstream filling of earth. Indeed,
352 for the first increments the displacements are directed towards upstream and from a certain point
353 on the sign of the displacement changes until the failure happens.

354 These swelling effects, related to the specific kind of analysis carried out, do not produce
355 significant variations on the reaching of the ultimate step and on the evaluation of the limit states.

356 **5 Conclusion**

357 This work is focused on the vulnerability analysis of the historical urban walls considering the
358 weakening effect induced by moisture.

359 The typical landslides analysis considers the effect of water only as an additional thrust and not
360 as a reduction of resistance in the soil or masonry. First of all, a model of imbibition is chosen in
361 order to evaluate the effect of moisture. Thanks to the combination of the models developed by
362 Montrasio and Yoshida, it is possible to consider the weakening effect induced by water for all
363 the soil types. In addition, a discretization of the soil in horizontal strata, both upstream and
364 downstream of the walls, allows to take into account more reliably the effect of imbibition in
365 depth.

366 This model is applied in retrospective to the real case of collapse of the Volterra's urban walls.
367 The properties of the materials are determined by accurate in situ surveys and the effect of this
368 model in the landslide vulnerability is considered with five imbibition scenarios and two kind of
369 analysis.

370 The Volterra case study shows a good sensibility of the results to imbibition and this can be
371 probably assumed as a significant contributing factor to the collapse of the section 92-93 in
372 January 2014.

373 The analysis, extended to other significant sections, allow to highlight the relevant effects of
374 imbibition on the vulnerability of urban walls. In particular, for the considered sections the return
375 periods of the rain induced by the four limit states are calculated.

376 The use of simplified models with the application of imbibition shows that in this case the LAM
377 method can provide useful indication in order to prevent collapse. This method can be applied
378 with a low information level and a reduced computational burden. For this reason, it is an
379 interesting manner to evaluate the most critical sections.

380 The analysis also highlights the relevant role of the limitation of the displacements as premonitory
381 signs of the collapse. The continuous check of the displacements to the head of the urban walls
382 allows to have at disposal an efficient early warning system as actually performed in Volterra.

383 **Data Availability**

384 Some or all data, models, or code that support the findings of this study are available from the
385 corresponding author upon reasonable request.

386 **Acknowledgement**

387 The Authors thank MIUR (Italian Ministry of University Research and Instruction) for financing
388 the MICHe (Mitigating the Impact of natural Hazard on Cultural Heritage, sites and artefacts)
389 Project with PRIN 2015 programme.

390 **References**

- 391 AA. VV., 2006. Linee seganalatrici di probabilità pluviometrica. PRESIDENZA DEL CONSIGLIO DEI
392 MINISTRI - DIPARTIMENTO PER I SERVIZI TECNICI NAZIONALI, Pisa.
- 393 Andreini, M., de Falco, A., Giresini, L., Sassu, M., 2013. Collapse of the historic city walls of Pistoia
394 (Italy): Causes and possible interventions. *Appl. Mech. Mater.* 351–352, 1389–1392.
395 <https://doi.org/10.4028/www.scientific.net/AMM.351-352.1389>
- 396 Borselli, L., 2018. SSAP2010 Slope Stability Analysis Program, Manuale di Riferimento.
- 397 Casapulla C., Maione A., 2017. Critical Response of Free-Standing Rocking Blocks to the Intense Phase
398 of an Earthquake. *Int. Rev. Civ. Eng.* 8.
- 399 Casapulla, C., 2015. On the resonance conditions of rigid rocking blocks. *Int. J. Eng. Technol.* 7, 760–771.
- 400 Casapulla, C., 2008. Lower and upper bounds in closed form for out-of-plane strength of masonry structures
401 with frictional resistances, in: *Structural Analysis of Historic Construction: Preserving Safety and*
402 *Significance - Proceedings of the 6th International Conference on Structural Analysis of Historic*
403 *Construction, SAHC08.* pp. 1191–1198.
- 404 Casapulla, C., Jossa, P., Maione, A., 2010. Rocking motion of a masonry rigid block under seismic actions:
405 a new strategy based on the progressive correction of the resonance response. *Ing. Sismica* 27, 35–
406 48.
- 407 Croce, P., Beconcini, M.L., Formichi, P., Landi, F., Puccini, B., Zotti, V., Bayesian methodology
408 for probabilistic description of mechanical parameters of masonry walls, *ASCE-ASME*
409 *Journal of Risk and Uncertainty in Engineering Systems, Part A: Civil Engineering, Vol 7*
410 (21), June 2021 Article number 04021008.
- 411 D.M. 17/01/2018, 2018. Aggiornamento delle “Norme Tecniche per le Costruzioni” (in italian).
- 412 Deere, D.U.. D.W., 1988. The rock quality designation (RQD) index in practice. *Symp. Rock Classif. Syst.*
413 <https://doi.org/10.1520/STP48465S>
- 414 Eurocode, C., 2004. 8: Design of structures for earthquake resistance—Part 1: General rules, seismic

415 actions and rules for buildings (EN 1998-1: 2004). Eur. Comm. Norm. Brussels 1.

416 Farooq, K., Rogers, J.D., Ahmed, M.F., 2015. Effect of Densification on the Shear Strength of Landslide
417 Material: A Case Study from Salt Range, Pakistan. *Earth Sci. Res.* 4, 113–125.
418 <https://doi.org/10.5539/esr.v4n1p113>

419 Franceschini, S., 2012. Analisi critica di modelli previsionali per le frane in Emilia Romagna. University
420 of Bologna. <https://doi.org/10.6092/unibo/amsdottorato/4731>

421 Fredlund, D., Rahardjo, H., 1993. Soil mechanics for unsaturated soils. *Soil Dyn. Earthq. Eng.* 12, 449–
422 450. [https://doi.org/10.1016/0267-7261\(93\)90011-F](https://doi.org/10.1016/0267-7261(93)90011-F)

423 Grillanda, N., Chiozzi, A., Bondi, F., Tralli, A., Manconi, F., Stochino, F., Cazzani, A., 2019. Numerical
424 insights on the structural assessment of historical masonry stellar vaults: the case of Santa Maria del
425 Monte in Cagliari. *Contin. Mech. Thermodyn.* 1, 24. [https://doi.org/https://doi.org/10.1007/s00161-](https://doi.org/https://doi.org/10.1007/s00161-019-00752-8)
426 [019-00752-8](https://doi.org/https://doi.org/10.1007/s00161-019-00752-8)

427 Losi, G.L., 2012. Modellazione spazio-temporale dei fenomeni di soil slip: dalla scala di pendio alla scala
428 territoriale. Università degli Studi di Parma.

429 Mistretta, F., Stochino, F., Sassu, M., 2019. Structural and thermal retrofitting of masonry walls: An
430 integrated cost-analysis approach for the Italian context. *Build. Environ.* 155, 127–136.
431 <https://doi.org/https://doi.org/10.1016/j.buildenv.2019.03.033>

432 Montrasio, L., Valentino, R., 2016. Modelling Rainfall-induced Shallow Landslides at Different Scales
433 Using SLIP - Part II. *Procedia Eng.* 158, 482–486. <https://doi.org/10.1016/j.proeng.2016.08.476>

434 Montrasio, L., Valentino, R., 2008. A model for triggering mechanisms of shallow landslides. *Nat. Hazards*
435 *Earth Syst. Sci.* 8, 1149–1159. <https://doi.org/10.5194/nhess-8-1149-2008>

436 Montrasio, L., Valentino, R., 2007. Experimental analysis and modelling of shallow landslides. *Landslides*
437 4, 291–296. <https://doi.org/10.1007/s10346-007-0082-3>

438 Montrasio, L., Valentino, R., Losi, G.L., 2009. Rainfall-induced shallow landslides: A model for the
439 triggering mechanism of some case studies in Northern Italy. *Landslides* 6, 241–251.
440 <https://doi.org/10.1007/s10346-009-0154-7>

441 Montrasio, L., Valentino, R., Terrone, A., 2014. Application of the SLIP Model. *Procedia Earth Planet. Sci.*
442 9, 206–213. <https://doi.org/10.1016/j.proeps.2014.06.023>

443 Puppio, M.L., Giresini, L., 2019. Estimation of tensile mechanical parameters of existing masonry through
444 the analysis of the collapse of Volterra's urban walls. *Frat. ed Integrita Strutt.* 13, 725–738.

445 <https://doi.org/10.3221/IGF-ESIS.49.65>

446 Puppio, M.L., Vagaggini, E., Giresini, L., Sassu, M., 2019. Large-scale survey method for the integrity of
447 historical urban walls : application to the case of Volterra (Italy), in: VECF1 - 1st Virtual European
448 Conference on Fracture. ELSEVIER B.V, pp. 1–14.

449 Santerecchi, E., 2014. Geologic and Geotecnic report - Volterra.

450 Sassu, M., Stochino, F., Mistretta, F., 2017. Assessment method for combine structural and energy
451 retrofitting in masonry buildings. Buildings 7.

452 Schilirò, L., Montrasio, L., Scarascia Mugnozza, G., 2016. Prediction of shallow landslide occurrence:
453 Validation of a physically-based approach through a real case study. Sci. Total Environ. 569–570,
454 134–144. <https://doi.org/10.1016/j.scitotenv.2016.06.124>

455 Vagaggini, E., 2019. Vulnerabilità di mura storiche urbane: il rischio frana perle mura di Volterra.

456 Valentino, R., Meisina, C., Montrasio, L., Losi, G.L., Zizioli, D., 2014. Predictive Power Evaluation of a
457 Physically Based Model for Shallow Landslides in the Area of Oltrepò Pavese, Northern Italy.
458 Geotech. Geol. Eng. 32, 783–805. <https://doi.org/10.1007/s10706-014-9758-3>

459 VV, A., n.d. Straus7 Reference Manual & User Guide.

460 Y.C. Chan, 1982. Study of old masonry retaining walls in Hong Kong. Hong Kong.

461 Yoshida, Y., Kuwano, J., Kuwano, R., 1991. Effects of Saturation on Shear Strenght of Soils. Soils Found.
462 31, 181–186.

463

464

N°	DATE	LOCATION	COLLAPSED PORTION	OBSERVED CAUSE	REPAIR COSTS
1	Sept. 2011	Pistoia	50 m	Poor masonry quality and low maintenance	1.500.000 €
2	Nov. 2012	Magliano in Toscana	30 m	Poor masonry quality and intense rainfall	980.000 €
3	Oct. 2013	Cana di Roccalbegna	13 m	Intense rainfall and low maintenance	170.000 €
4	Jan. 2014	Volterra	35 m	Intense rainfall and poor drainage system	1.500.000 €
5	Mar. 2014	Volterra	20 m	Intense rainfall and low maintenance	500.000 €
6	Dec. 2014	Magliano in Toscana	15 m	Poor masonry quality and low maintenance	300.000 €
7	Apr. 2018	San Gimignano	20 m	Intense rainfall	500.000 €

465

Tab. 1 – Extension, estimated cause of collapse and repairing costs (Puppio et al., 2019).

466

467

Lithotype	ϕ [°]	c' [kPa]	γ [kN/m ³]	γ_{sat} [kN/m ³]
Sand – Villamagna formation	37	0	20	22
Lime soil	15	20	17	18

468

Tab. 2 – Geotechnical parameters of the soil.

469

d_{SLCg}	d_{SLV}	d_{SLD}	d_{SLI}
Incipient collapse	$0.9 \times d_{SLCg}$	$h_w / 100$	Expert Judgement

470

Tab. 3 - Limit states.

471

$T_r = 175$ years

Units

t	0	1	3	6	12	24	[hours]
h	0	82	109	121	158	190	[mm]
m	0	0,31	0,41	0,49	0,59	0,7	-
S_r	0,3	0,51	0,58	0,64	0,71	0,79	-
c_w	10,4	3	1,8	1,1	0,5	0,2	[kPa]
ϕ	37	27,5	26	24,5	24	22,5	°
γ^*	20	20,65	20,86	21	21,21	21,44	[kN/m ³]

472

Tab. 4 – Saturation coefficients Vs duration t of rain (hours).

	Materials	γ (kg/m³)	E (kPa)	Φ (°)	c (kPa)
1.	Filling masonry	1900	1200000	44	410
2.	Masonry	2100	1200000	44	410
3.	Sand (Villamagna Formation)	2000	23076	37	10,4
4.	Lime soil	1700	16240	15	20

473

Tab. 5 - Material properties according to the Mohr-Coulomb criterion.

474

Layer	Sr [%]	γ [kg/m^3]	c [kN/m^2]	ϕ [$^\circ$]
(t = 0)	30	20	10,4	37
(t = 1 hour)	51	20,65	3	27,5
(t = 3 hours)	58	20,86	1,8	26
(t = 6 hours)	64	21	1,1	24,5
(t = 12 hours)	71	21,21	0,5	24
(t = 24 hours)	79	21,44	0,2	22,5

475

Tab. 6 - Mechanical parameters of the soil with $T_r=175$ Years.

476

Section	Limit State	<i>Tr</i> [years]	<i>h_C</i> [m]	<i>Pns</i> [%]
92-93	SLI	10	0,085	0%
	SLD	75	0,159	37%
	SLV	175	0,175	65%
	SLC	658	0,205	89%
32-33	SLI	10	0,085	0%
	SLD	466	0,196	85%
	SLV	658	0,212	89%
	SLC	740	0,217	90%
48-49	SLI	10	0,085	0%
	SLD	76	0,159	37%
	SLV	404	0,190	83%
	SLC	430	0,193	84%
71-72	SLI	10	0,085	0%
	SLD	401	0,190	83%
	SLV	593	0,207	88%
	SLC	658	0,212	89%

Tab. 7 – Results for the analyzed section from FEM Model. The analysis is referred to a rainfall duration of 12 hours.



Fig. 1 – Failure cases analysed in Tuscany (adapted from Puppino et al., 2019).

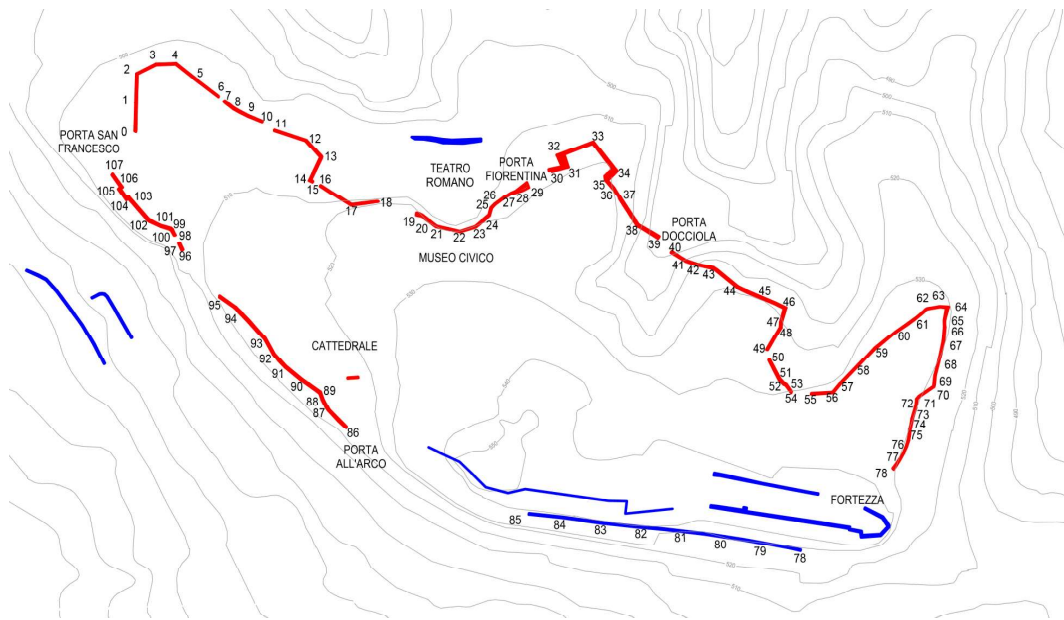


Fig. 2 - Perimeter of the urban walls of Volterra from GIS survey (adapted from Puppio et al., 2019). In red the Medieval part and in blue the Etruscan part.



Fig. 3 - Perimeter of the surveyed urban walls of Volterra overlaid on an aerial view (adapted from Puppio et al., 2019).



Fig. 4 - Presence of moisture before the collapse of January 2014 of the Urban walls of Volterra.



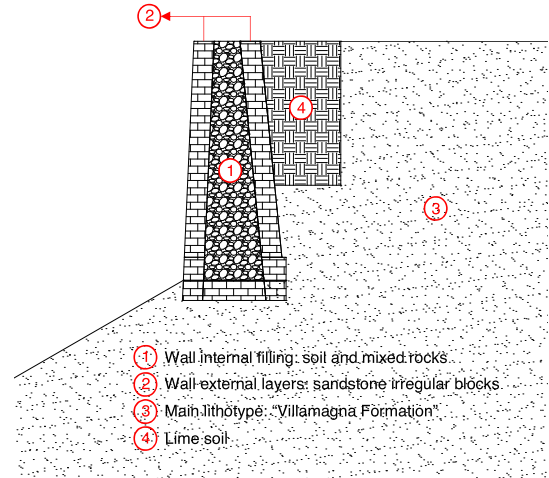
(a)

(b)

Fig. 5 – Views of the collapsed area: (a) natural gas pipeline under the road, (b) foundation of Palazzo Stella.



(a)



(b)

Fig. 6 – (a) Picture of the wall after the collapse - (b) main soil lithotypes and wall layers.



(a)



(b)

Fig. 7 - Drilling with SPT test: (a) location - (b) coring samples (adapted from Santarecchi, 2014).

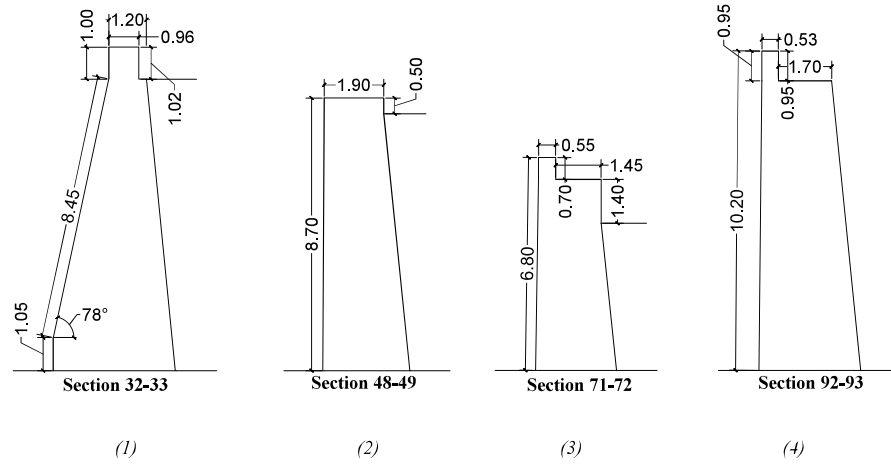


Fig. 8 - Main vertical sections analysed. Units in meters.

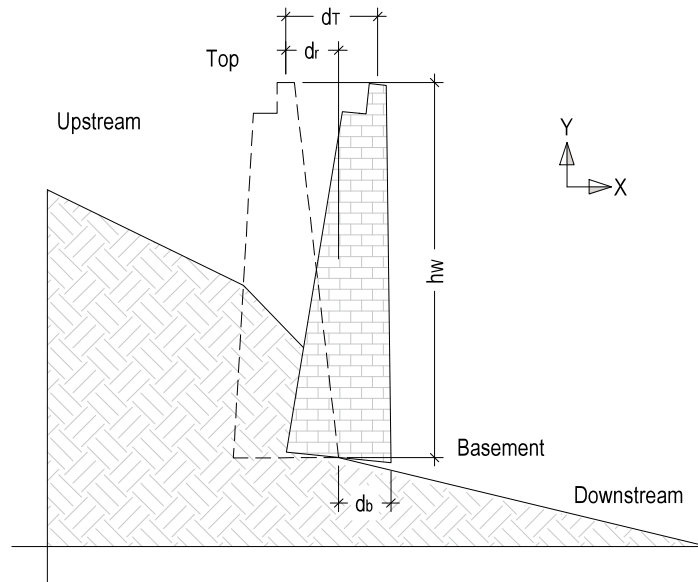


Fig. 9 – Relative displacements.

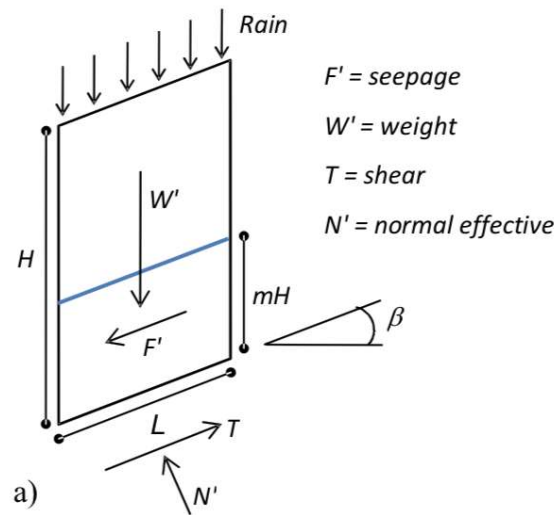


Fig. 10 – View of imbibition level for the Slip model.

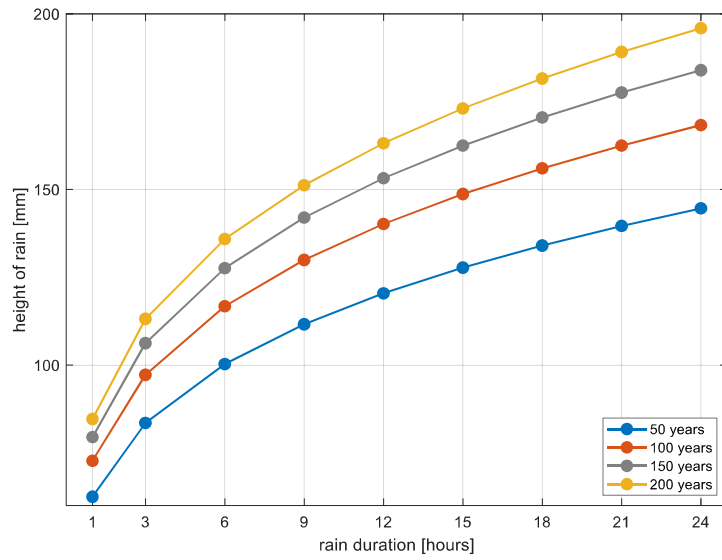


Fig. 11 – The return period of the Volterra site in terms of rainfall intensity (adapted from AA. VV., 2006).

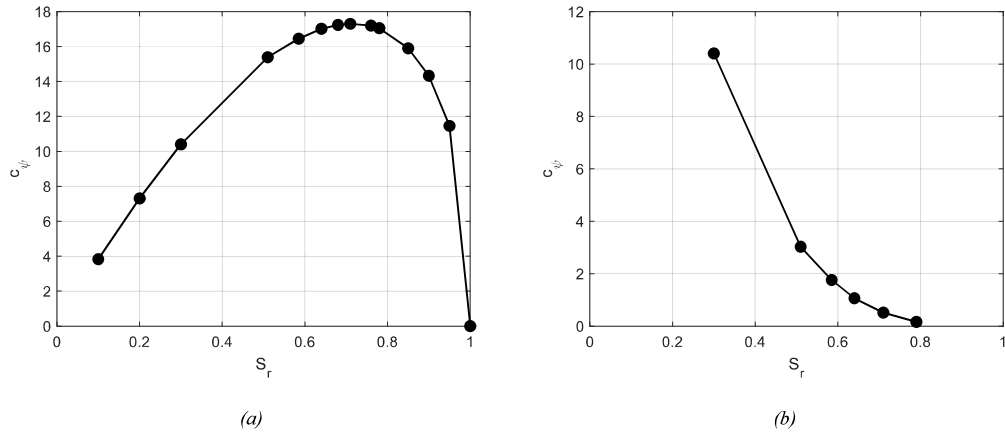


Fig. 12 – Apparent cohesion c_ψ vs saturation grade S_r , for the state mH (a) and for the entire deep H (b).

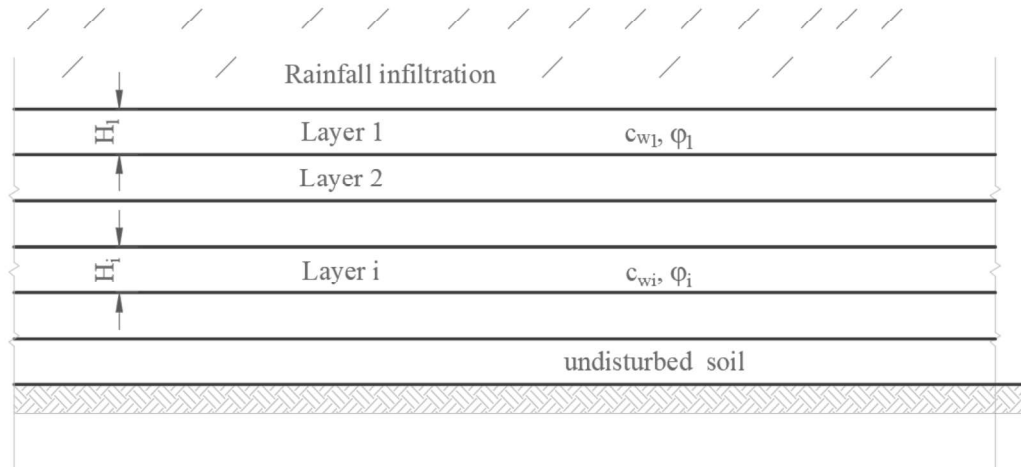


Fig. 13 – Vertical section of the soil with discretization in horizontal layers.

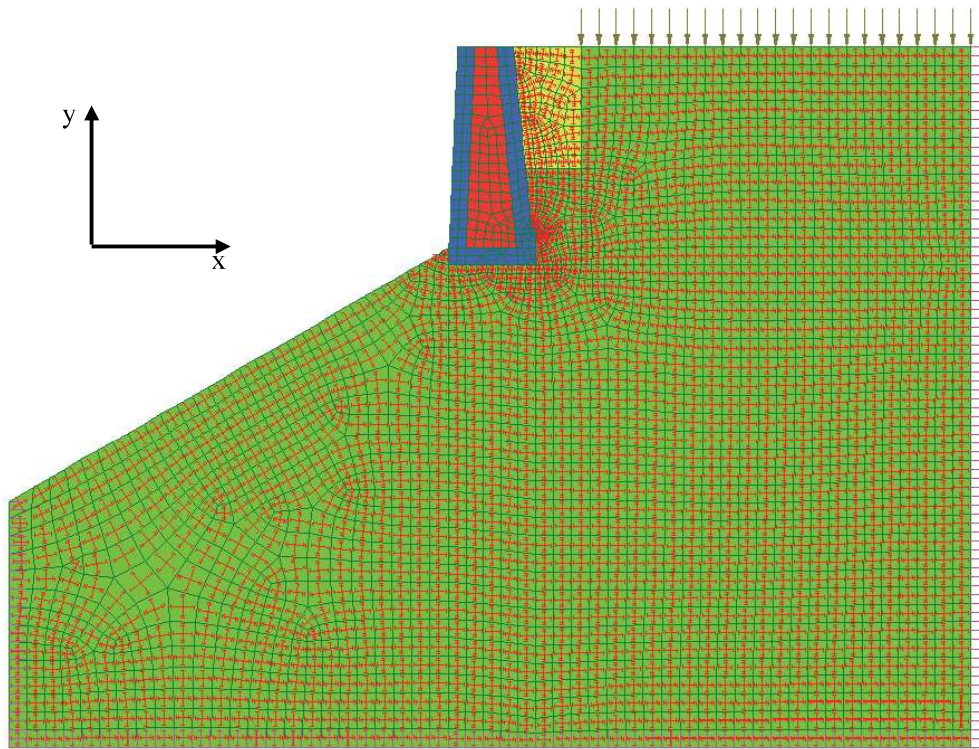


Fig.14 – Model of the section 92-93 (Straus7). The mesh is more accurate in which stress concentrations are expected.

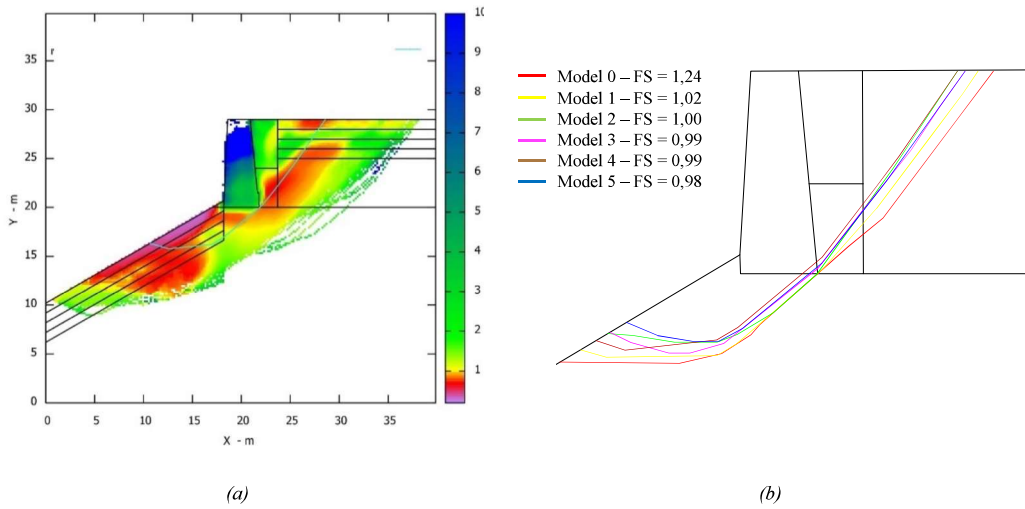


Fig. 15 – LAM of section (92-93) code SSAP2010 (Borselli, 2018); safety factors (a) and slip surfaces (b).

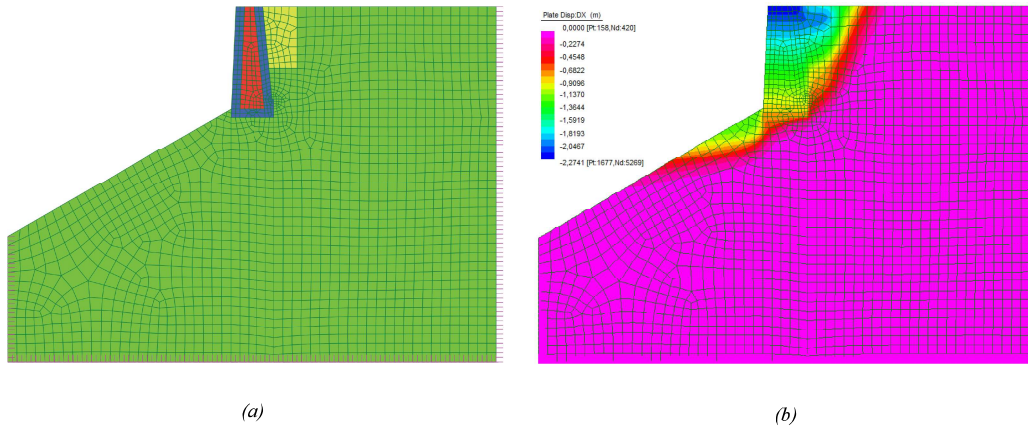


Fig. 16 – FEM Analysis of section (92-93); geometry and mesh (a); horizontal displacements (b).

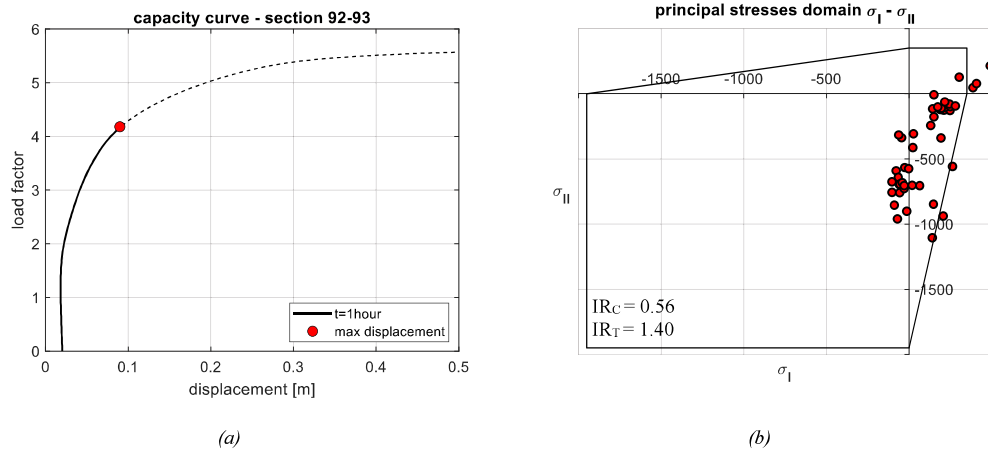


Fig. 17 – Pushover (a) and principal stresses domain (b) for a rain duration of 1 hour.

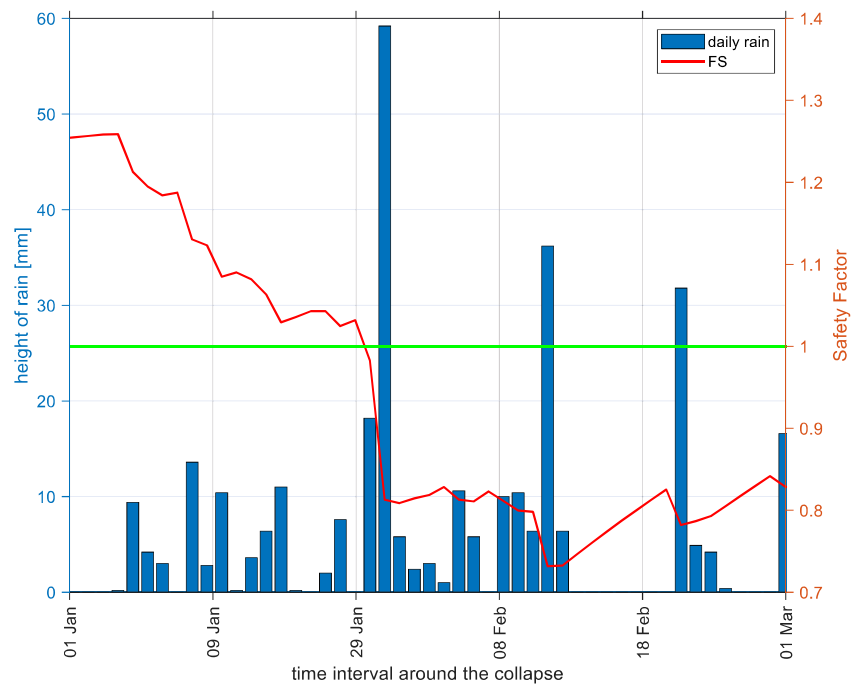
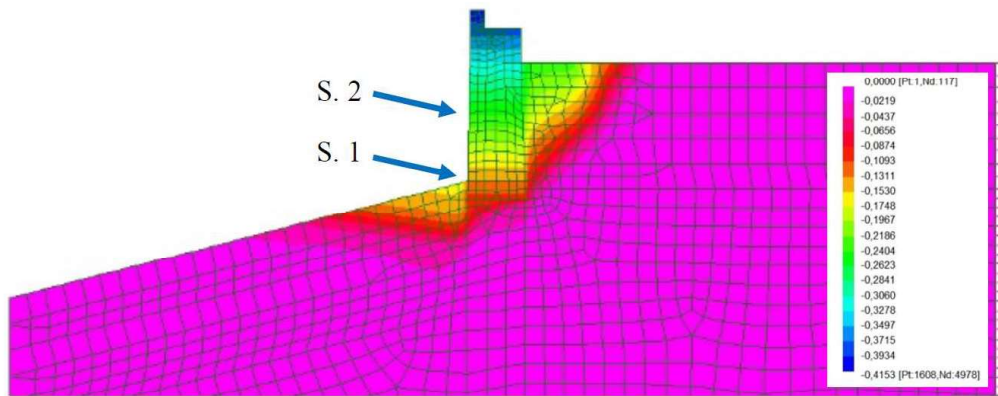
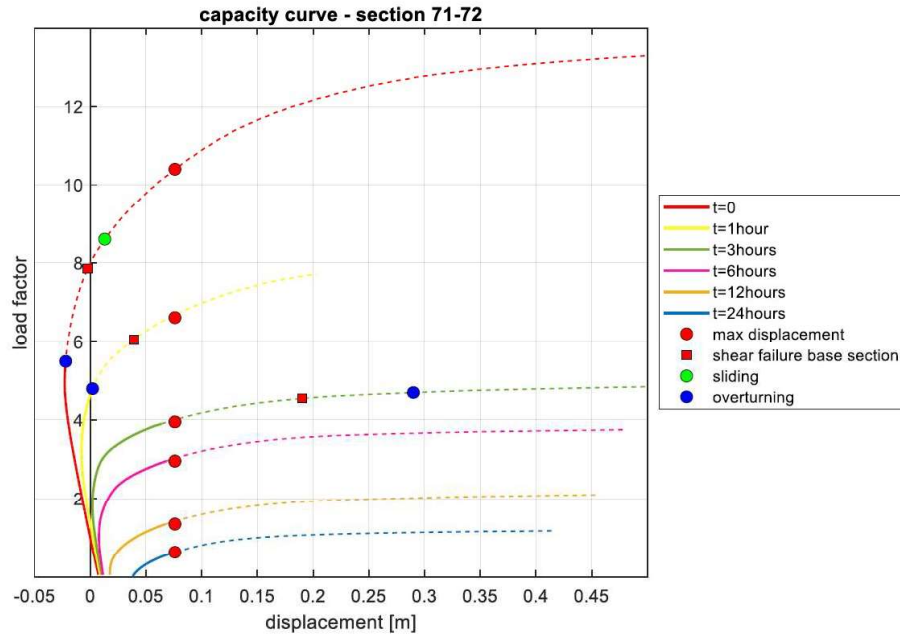


Fig. 18 – Sensitivity analysis of the effect of imbibition with the real rainfalls registered in the days around the collapse (30th January 2014).

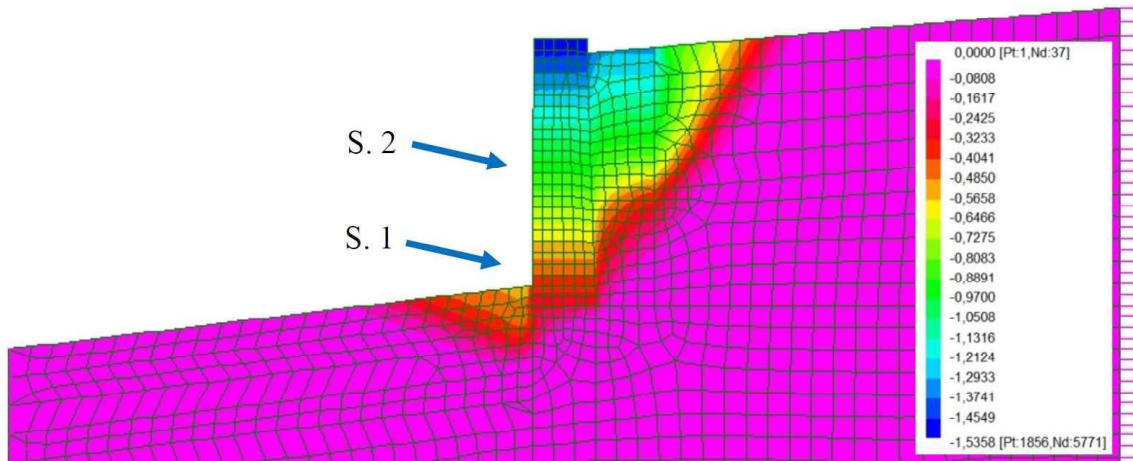


(a)

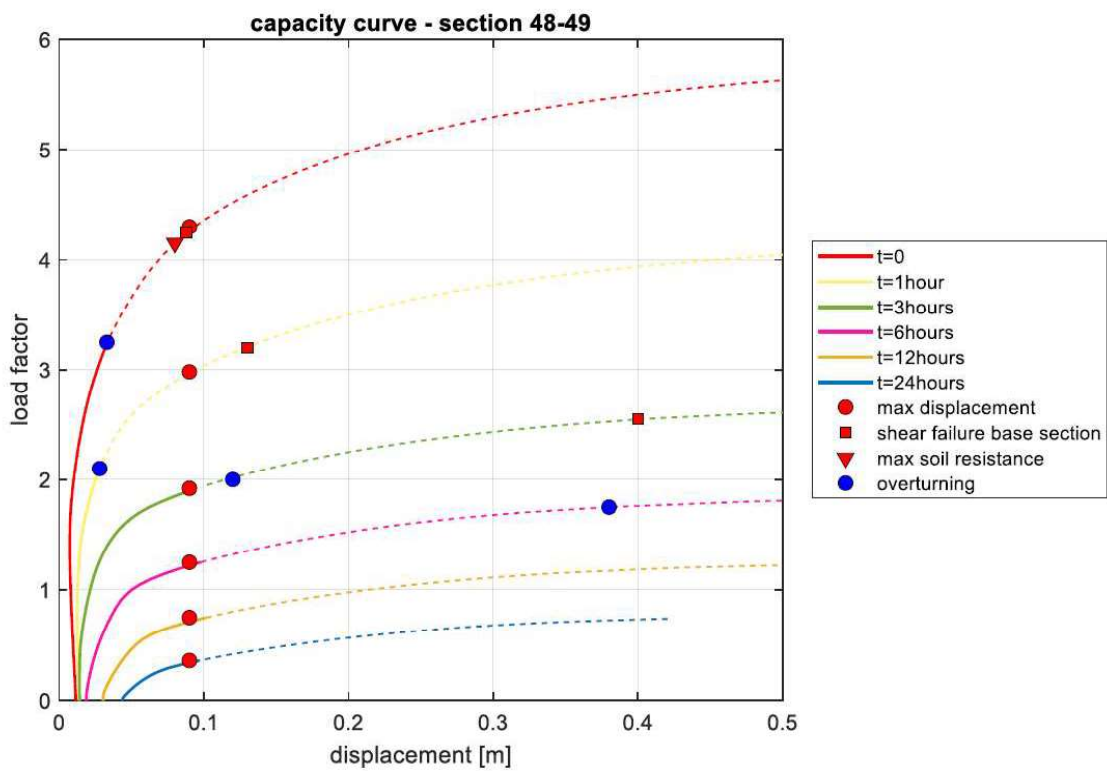


(b)

Fig. 19 – Section 32-33, (a) contour of the horizontal displacement [m] of model 5 and (b) results of the pushover curves for all the models.

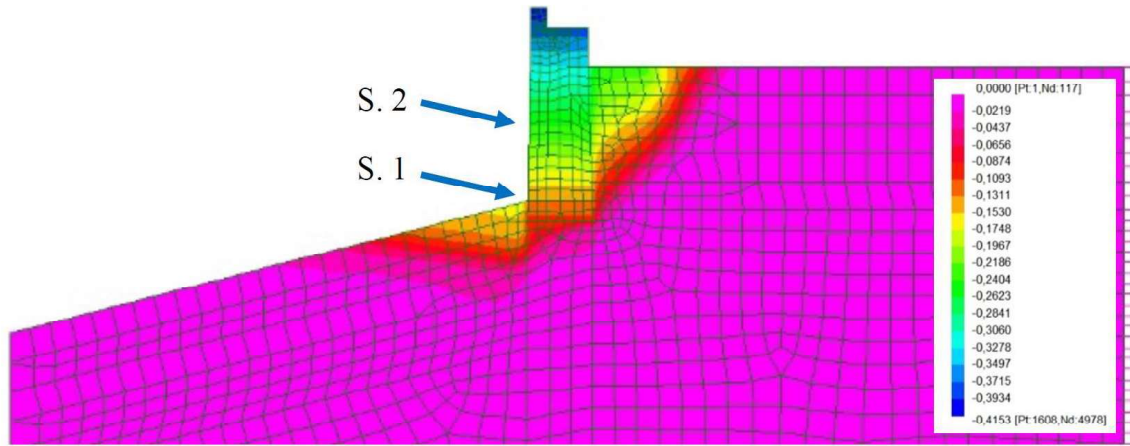


(a)

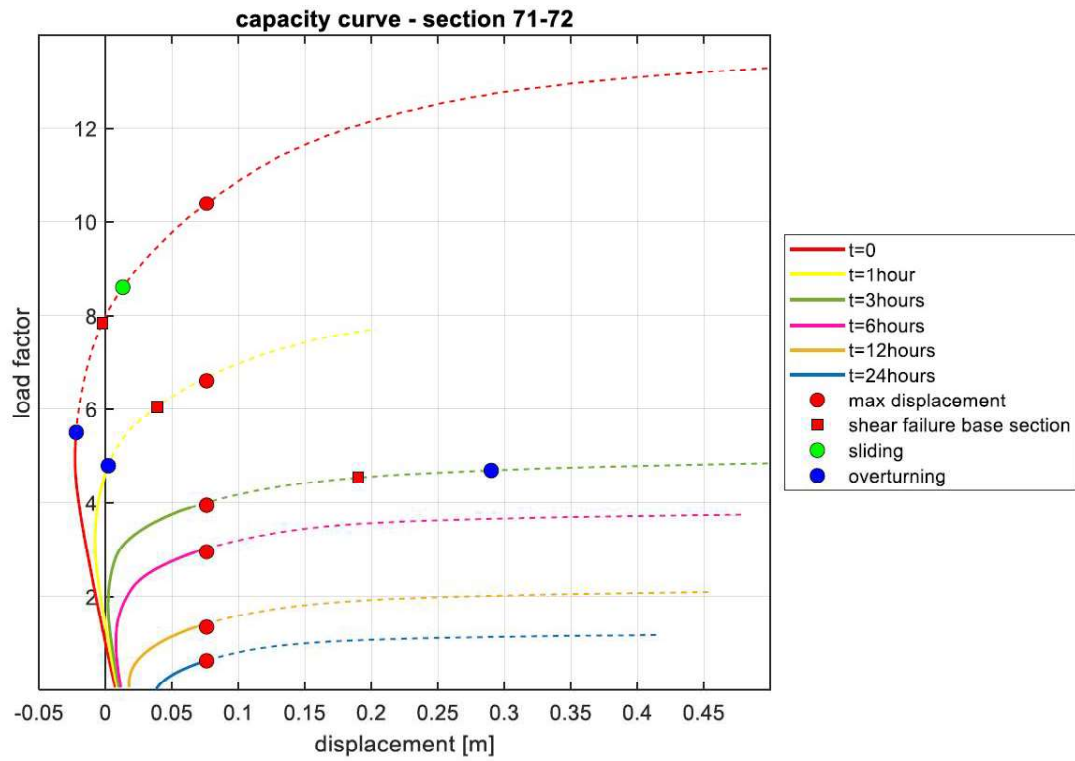


(b)

Fig. 20 – Section 48-49, (a) contour of the horizontal displacement [m] of model 5 and (b) results of the pushover curves for all the models.



(a)



(b)

Fig. 21 – Section 71-72, (a) contour of the horizontal displacement [m] of model 5 and (b) results of the pushover curves for all the models.